Case Report

Advanced magnetic resonance imaging findings of cerebellar hemangioblastomas: A report of three cases and a literature review

Eiji Matsusue[1] , Chie Inoue[1], Sadaharu Tabuchi[2], Hiroki Yoshioka[2], Yuichiro Nagao[2], Kensuke Matsumoto[1], Kazuhiko Nakamura[1] and Shinya Fujii[3]

Abstract

On conventional magnetic resonance imaging (MRI), hemangioblastomas typically appear as mural nodules with an adjacent surrounding cyst or a solid mass in the cerebellum. However, hemangioblastomas sometimes cannot be reliably distinguished using this imaging technique from other tumors, especially pilocytic astrocytomas and metastatic tumors, because of their similar imaging findings and locations. Herein, we report three cases of cerebellar hemangioblastomas and review their findings on conventional and advanced MRI, including diffusion-weighted imaging (DWI), dynamic susceptibility-weighted contrast-enhanced perfusion-weighted imaging (DSC-PWI), and magnetic resonance spectroscopy (MRS). Solid contrast-enhanced lesions of hemangioblastomas showed increased apparent diffusion coefficient values on DWI, increased relative cerebral blood volume ratio on DSC-PWI, and high lipid/lactate peak on MRS. Therefore, advanced MRI techniques can be helpful in understanding the pathological and metabolic changes of hemangioblastomas and may be useful for their characterization.

Introduction

Hemangioblastomas (HBs) are classified as Grade I, mesenchymal, and non-meningothelial tumors according to the World Health Organization's classification of central nervous system tumors.[1] They represent 1.5–2.5% of all intracranial neoplasms and 7–12% of posterior fossa tumors. Additionally, HBs are most frequently present in the cerebellar hemisphere and in individuals in their third to fifth decades of life.[2] Moreover, 20% of cases are associated with Von Hippel–Lindau (VHL) disease.[3] According to symptomatology, the condition is dominated by cerebellar signs of ataxia, dizziness, headache, and intracranial hypertension, which are strongly associated with tumor size and cyst mass effect.[2,4] Histologically, HBs are characterized by

stromal cells with plump foamy cytoplasm and an abundant capillary network.[2] HBs are subclassified into reticular and cellular variants.[2,5] Most HBs are the reticular variant,

[1]Department of Radiology, Tottori Prefectural Central Hospital, Tottori, Japan
[2]Department of Neurosurgery, Tottori Prefectural Central Hospital, Tottori, Japan
[3]Division of Radiology, Department of Multidisciplinary Internal Medicine, Tottori University, Tottori, Japan

Corresponding author:
Eiji Matsusue, Department of Radiology, Tottori Prefectural Central Hospital, 730 Ezu, Tottori 680-0901, Japan.
Email: matsusuee@tp-ch.jp

which shows abundant capillaries and stromal cells. The cellular variant is less common than the reticular variant and is predominantly composed of densely packed stromal cells. On conventional magnetic resonance imaging (MRI), HBs typically appear as mural nodules with an adjacent non-enhancing surrounding cyst or solid and internal and/or peripheral vessels located in the cerebellum.[6,7] However, they sometimes cannot be reliably distinguished from other tumors by conventional MRI, especially pilocytic astrocytomas (PAs) in adolescents[8] and metastatic brain tumors (Mets) in adults,[9] because of their similar imaging findings and locations. The application of advanced MRI techniques, including diffusion-weighted imaging (DWI),[9–12] dynamic susceptibility-weighted contrast-enhanced perfusion-weighted imaging (DSC-PWI),[8,9,11,13–15] and proton magnetic resonance (MR) spectroscopy (MRS),[8,16,17] has a better chance of assessing and distinguishing the functional and metabolic differences between HBs and other tumors. We present three cases of HB and review their findings on conventional and advanced MRI, including DWI, DSC-PWI, and MRS.

Case history

Case 1

A 35-year-old woman presented with a chief complaint of headache lasting for 2 months. Conventional MRI showed a cystic mass lesion with a mural nodule in the left cerebellar hemisphere. The mural nodule appeared as high signal intensity on T2-weighted images (T2WI) and was associated with flow voids. Moreover, the nodule was homogeneously enhanced, although the cyst wall was not enhanced. The apparent diffusion coefficient (ADC) of the nodule was 1.6×10^{-3} mm^2/s. DSC-PWI showed an elevated regional cerebral blood volume (rCBV) ratio; that is, the maximal rCBV value (enhanced lesion)/the rCBV value (contralateral normal white matter) was 12.42. The intensity–time curve showed only a partial return to the baseline level due to massive leakage of contrast media into the interstitial space (Figure 1). The differential diagnoses included HB, Mets, PA, and pleomorphic xanthoastrocytoma.

Case 2

A 32-year-old woman presented with headache, dizziness, and sensory disorders of the bilateral lower limbs. Conventional MRI revealed a nodular lesion in the left cerebellar hemisphere. The nodule appeared as slightly high signal intensity on T2WI and was associated with perifocal edema. Additionally, the nodule was homogeneously enhanced, with an ADC value of 1.3×10^{-3} mm^2/s. The DSC-PWI showed increased CBV of the nodule (Figure 2), but the value could not be determined. Proton MRS with a short echo time (TE) was performed using a 3T system. The

sequence, repetition time, TE, and measurement frequency were point-resolved spectroscopy, 2000 ms, 36 ms, and 128 times, respectively. A single voxel measuring $16 \times 25 \times 21$ mm was set up, which included the edematous cerebellar region around the cerebellar enhanced nodule (Figure 2). Proton MRS revealed slightly increased lipids and/or lactate peak (Lip/Lac) between 0.9 and 1.4 ppm. The other spectra were almost normal (Figure 2). The spectra obtained from the voxel that included the edematous cerebellar parenchyma around the enhanced lesion may have reflected the tumor as well as a large part of the normal tissue. Five months later, both the nodule and perifocal edema appeared slightly enlarged on MRI. The differential diagnoses included HB, Mets, PA, and small vascular malformations.

Case 3

An 84-year-old man complained of dysarthria and light-headedness while walking. MRI revealed a mass lesion in the left cerebellar hemisphere. The lesion appeared as high signal intensity on T2WI and was associated with flow voids. Moreover, the lesion was homogeneously enhanced, and DWI showed that the mass was of low intensity. The ADC value of the nodule was 2.3×10^{-3} mm^2/s. The DSC-PWI showed an elevated rCBV ratio, that is, the maximal rCBV value (enhanced lesion)/the rCBV value (contralateral normal white matter) was 12.27. The intensity–time curve showed only a partial return to the baseline level, as seen in Case 1 (Figure 3). Proton MRS with a short TE was performed using a 3T system. A single voxel of size $16 \times 20 \times 15$ mm was set up within the mass lesion (Figure 3). The spectra obtained from the voxel that included the entire enhanced lesion reflected the tumor lesion without necrosis. MRS revealed prominent Lip/Lac between 0.9 and 1.4 ppm. Other spectra, including choline (Cho), n-acetylaspartate (NAA), and creatine peak (Cr), were almost absent (Figure 3). The differential diagnoses included HB and Mets.

A summary of the clinical data, MRI, and MRS findings for these three cases with HBs is shown in Table 1. In all cases, the tumors were completely excised and the histological diagnosis was HBs. The stromal cells were positive for inhibin-α, D2-40, and S100 in immunohistochemistry tests. VHL disease was ruled out by chest and abdominal computed tomography and fundoscopic examination in each case. The postoperative course was uneventful in all cases.

Discussion

The most common conventional MR patterns of HBs are traditionally described as enhanced mural nodules with adjacent non-enhanced surrounding cysts or enhanced solid lesions.[7] Furthermore, HBs commonly (60–69% of cases) have associated internal and/or peripheral signal flow voids, consistent with the pathologically identified dilated afferent
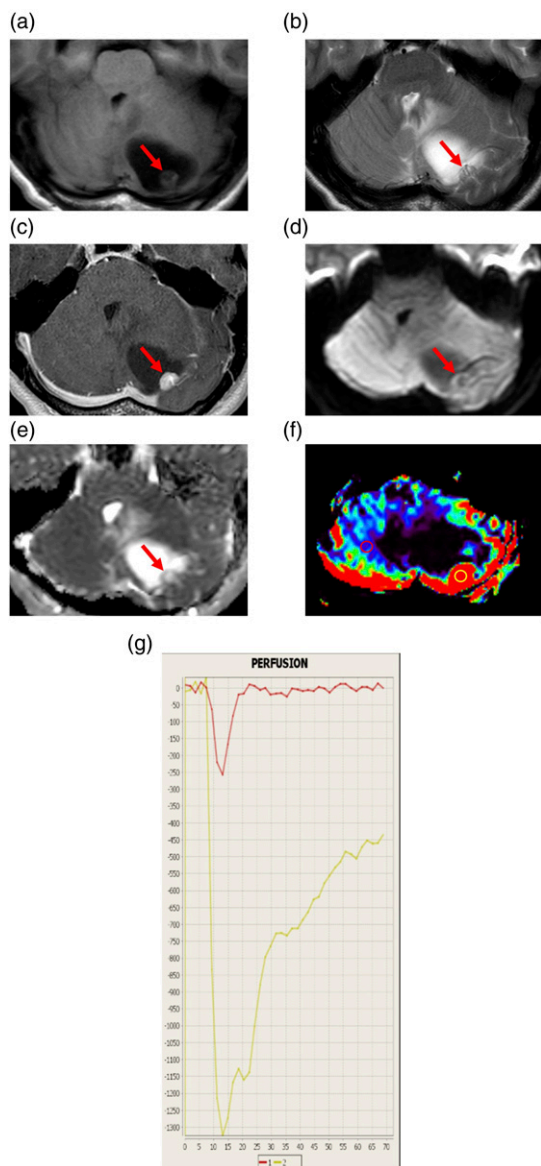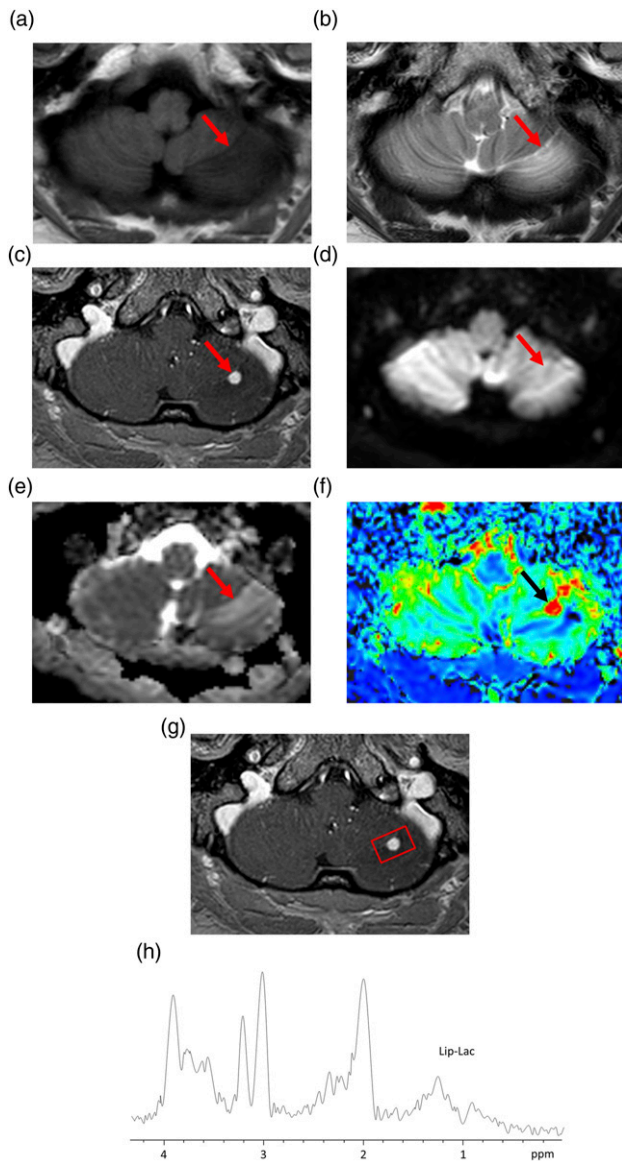
Figure 1. Representative magnetic resonance imaging findings of a 35-year-old woman with hemangioblastoma (Case 1). (a) Axial T1-weighted image (T1WI) showing a cystic mass lesion with a mural nodule in the left cerebellar hemisphere. The cystic lesion is low-intense, while the nodule (arrow) is slightly low-intense compared to the cerebellum. (b) Axial T2WI showing flow voids (arrow) in the mural nodule. (c) Axial contrast-enhanced T1WI showing homogeneous enhancement of the mural nodule (arrow) and no enhancement of the cyst wall. (d) Axial diffusion-weighted image showing that the mural nodule (arrow) is low-intense. (e) A corresponding apparent diffusion coefficient (ADC) map showing increased ADC of the nodule (arrow). The ADC value is 1.6×10^{-3} mm^2/s. (f) Relative cerebral blood volume (rCBV) map showing increased relative CBV (rCBV) of the nodule. The rCBV ratio, defined as the maximal rCBV (enhanced lesion in yellow circle)/rCBV (contralateral normal white matter in red circle), is 12.42. (g) The intensity–time curve showing only a partial return to the baseline level (yellow line) due to massive leakage of contrast media into the interstitial space.

and efferent vessels.[6,7] Traditionally, HBs have been classified into four morphologic patterns based on macroscopic pathology.[18] A cyst with a mural nodule type was the most common (60%), followed by a solid tumor type (26%) and a solid tumor with internal small cysts (9%), whereas a simple cyst type was the least common (5%). However, a literature review of 207 articles including 1759 infratentorial HBs over 31 years[19] reported the solid tumor type to be the most common (47.7%), followed by the cystic (26.3%) and cystic with a mural nodule (21.3%) types. Both solid and cystic types were the least common (4.7%). Regarding the cystic component of HBs, the cyst wall is normally not neoplastic and does not show enhancement on MRI.[20] However, there are some rare cases of HBs associated with an enhanced cystic wall, which were confirmed by histopathologic examination.[21–23] In addition, some cases of HB with MR non-enhanced neoplastic cyst walls have been reported.[24] In our cases, an enhanced mural nodule with an adjacent non-enhanced surrounding cyst (Case 1) and purely enhanced solid lesion (Cases 2 and 3) showed the common conventional MR patterns of HBs. Internal and peripheral signal flow voids were also observed in Cases 1 and 3.

MR measurement of the rCBV derived from DSC-PWI is a useful parameter for evaluating angiogenesis in HBs. A prominent elevation of rCBV has been reported in HBs.[9,11,13-15] HBs have abundant vessels within tumors due to the overexpression of vascular endothelial growth factor,[2] which causes a prominent increase in rCBV.

rCBV ratios ranging from 7.7 to 16.65 for cerebellar HBs have been reported.[9,11,13–15] In our cases, the rCBV ratios calculated from the solid contrast-enhanced portion were 12.42% and 12.27% in Cases 1 and 3, respectively. While the small nodular enhanced lesion in Case 2 also showed increased rCBV, the value was not determined. The prominent elevations of the rCBV ratios in our cases were consistent with previous observations in HBs.

DWI has been widely used for the evaluation of brain tumors. The ADC values represent the mobility of free water molecules within tissues and appear to be correlated with tumor cellularity. The ADC values for most cerebellar tumors, including Mets, are similar to or lower than those of the cerebellar parenchyma.[10,25] In contrast, increased ADC has been reported in cerebellar HBs, with values in the range of $1.27–1.55 \times 10^{-3}$ mm^2/s.[9–11,26] HBs are characterized by the presence of a network of capillary-like channels separated by stromal cells. The increased ADC values could be attributed to the high vascular spaces of capillaries as well as low cellular attenuation in HBs.[9,10] In contrast, cellular variants of HBs showed reduced ADC values, which may reflect the hypercellularity of stromal cells with fewer capillaries.[27] In our cases, the ADC values obtained from the solid contrast-enhanced portion were 1.6×10^{-3} mm^2/s, 1.3×10^{-3} mm^2/s, and 2.3×10^{-3} mm^2/s in Cases 1, 2, and 3, respectively. The differences in ADC may have resulted

Figure 2. Representative magnetic resonance imaging and magnetic resonance spectroscopy findings of a 32-year-old woman with hemangioblastoma (Case 2). (a) Axial T1-weighted image (T1WI) showing a low-intensity edematous lesion in the left cerebellar hemisphere. The nodular lesion (arrow) is unclear. (b) Axial T2WI showing a slight high-intensity nodule (arrow) with perifocal edema. (c) Axial contrast-enhanced T1WI (CE-T1WI) showing homogeneous enhancement of the nodule (arrow). (d) Axial diffusion-weighted image showing that the nodule is unclear (arrow). (e) A corresponding apparent diffusion coefficient (ADC) map showing slightly increased ADC of the nodule (arrow). The ADC value is 1.3×10^{-3} mm^2/s. (f) Relative cerebral blood volume (rCBV) map showing increased rCBV. (g) The volume of interest (VOI) for magnetic resonance spectroscopy with short echo time (36 ms) in axial CE-T1WI (square). The VOI includes the edematous cerebellar region around the cerebellar tumor nodule. The VOI measures 16 × 25 × 21 mm. (h) The spectra showing slightly increased lipid and/or lactate peak. Other spectra, including choline, n-acetylaspartate, and creatine peaks, are almost normal.
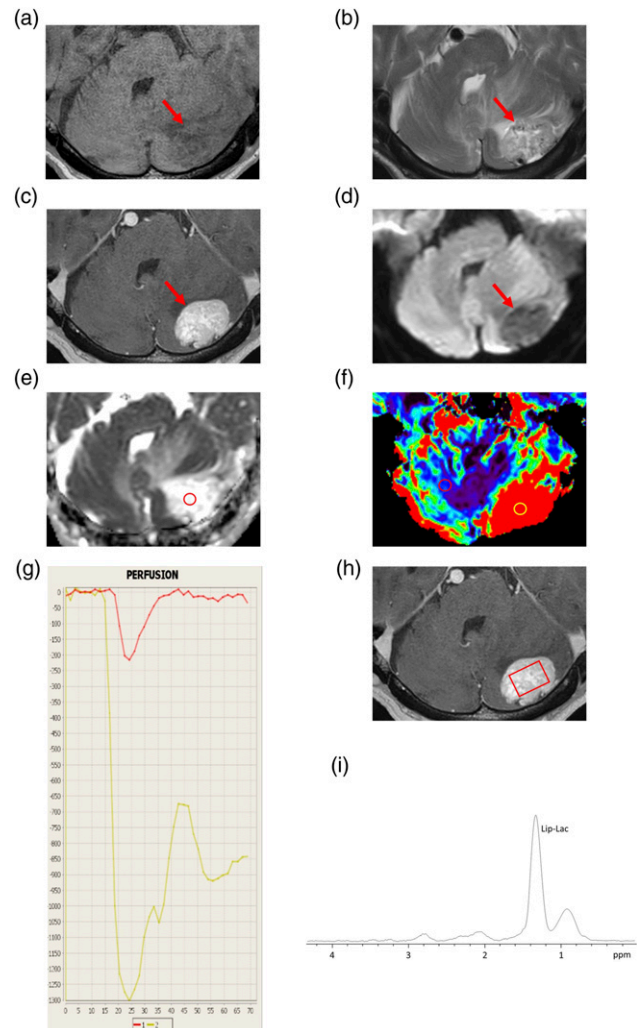
Figure 3. Representative magnetic resonance imaging and magnetic resonance spectroscopy findings of an 84-year-old man with hemangioblastoma (Case 3). (a) Axial T1-weighted image (T1WI) showing a homogenous low-intense mass lesion (arrow) in the left cerebellar hemisphere. (b) Axial T2WI showing flow voids (arrow) in the mass lesion with perifocal edema. (c) Axial contrast-enhanced T1WI (CE-T1WI) showing homogeneous enhancement of the mass lesion (arrow). (d) Axial diffusion-weighted image (DWI) showing the low-intensity mass lesion (arrow). (e) A corresponding apparent diffusion coefficient (ADC) map showing increased ADC of the nodule. The ADC value of the circle is 2.3×10^{-3} mm^2/s. (f) Relative cerebral blood volume (rCBV) map showing increased CBV. The rCBV ratio, defined as the maximal rCBV (enhanced lesion—yellow circle)/rCBV (contralateral normal white matter—red circle) is 12.27. (g) The intensity–time curve showing only a partial return (yellow line) to the baseline level due to massive leakage of contrast media into the interstitial space. (h) The volume of interest (VOI) for magnetic resonance spectroscopy with short echo time (36 ms) in the axial CE-T1WI (square). The VOI includes the entire enhanced lesion without necrosis. The VOI measures 16 × 20 × 15 mm. (i) The spectra showing prominent lipid and/or lactate peaks. Other spectra, including choline, n-acetylaspartate, and creatine peaks, are almost absent.

Table 1. Summary of the clinical data and MRI and MRS findings for cerebellar hemangioblastomas.

Case	Age/sex	Clinical presentation	Ope	VHL findings	IH	Conventional MRI findings	ADC map/ ADC value (10^{-3} mm^2/s)	rCBV map/ rCBV ratio	Lip-lac	Cho NAA Cr
1	35/F	· Headache	TR	Negative	Inhibin-α D2-40	Cyst with nodule with FV	Increased/1.6	Increased/ 12.42	NA	NA NA NA
2	32/F	· Headache · Dizziness · Sensory disorders	TR	Negative	Inhibin-α S100	Solid nodule without FV	Increased/1.3	Increased/ NA	+	+ + +
3	84/M	· Dysarthria · Lightheadedness	TR	Negative	Inhibin-α S100	Solid mass with FV	Increased/2.3	Increased/ 12.27	+ +	− − −

MRI: magnetic resonance imaging; MRS: magnetic resonance spectroscopy; Ope: operation; VHL: Von Hippel–Lindau disease; IH: positive immuno-histochemistry tests for stromal cells; ADC: apparent diffusion coefficiency; rCBV: relative cerebral volume; Lip-Lac: lipid and/or lactate; Cho: choline; NAA: N-acetylaspartate; Cr: creatine; FV: flow void; TR: total resection; NA: not available; +: present; + +: elevated; –: absent.

Table 2. Comparisons of general imaging features of hemangioblastomas, pilocytic astrocytomas, and metastatic tumors on conventional and advanced MRI.

	Hemangioblastomas	Pilocytic astrocytomas	Metastatic tumors
Age	Adults	Children	Adults
Morphology	Cyst with a mural nodule, solid, cyst, solid and cyst	Cyst with a mural nodule, Solid	Solid with necrosis
Number	Single	Single	Multiple > single
Flow voids	+	−	+
rCBV	Prominent increased	Mild increased	Mild to prominent increased
ADC	Increased	Iso to increased	Decreased to mild increased
Lip/Lac	+ (Lip)	+ (Lac)	+ (Lip/Lac)
Cho	− or +	++	++
NAA	−	+	−

MRI: magnetic resonance imaging; rCBV: cerebral blood volume; ADC: apparent diffusion coefficiency; Lip/Lac: lipid and/or lactate; +: present; Cho: choline; - : absent; + +: elevated; NAA: N-acetylaspartate.

from the differences in their histologic findings, especially those predominantly composed of capillaries or stromal cells in HBs.

MRS provides complementary metabolic and histologic marker information about brain tumors that could help in distinguishing brain tumors and tumor grading.[28,29] However, few studies have examined the MRS findings of cerebellar HBs. Prominent Lip, low creatine (Cr), absence of N-acetylaspartate (NAA), and increased choline (Cho) in HBs have been reported.[8,16,17] The presence of Lip/Lac may be associated with lipid droplets contained in the stromal cells of HBs.[2,8] Both Cases 2 and 3 showed increased Lip/ Lac on MRS. In Case 3, prominent Lip/Lac and almost absent NAA, Cr, and Cho were observed. In brain tumors, the presence of Lip/Lac often indicates the presence of necrotic tissue, which is an indicator of malignancy and poor prognosis.[30,31] However, in Case 3, the spectra obtained from a voxel that included the entire enhanced lesion reflected the tumor lesion without necrosis. Several reports have shown prominent Lip/Lac for tumors without central necrosis in PAs, malignant lymphoma, meningioma, and HBs. The prominent Lip/Lac of 1.3 ppm, which is observed in malignant lymphoma, meningioma, and HBs, mainly corresponds to the Lip, whereas in PAs, it is mainly the Lac.[8,32,33] Hence, a high Lip/Lac without a necrotic component on MRS is not specific but could be a characteristic finding of HBs and may play an important role in the differential diagnosis of cerebellar tumors.

The differential diagnoses of cerebellar HBs include PAs,[8,12,14,15] Mets,[9,11] arterial-venous malformation (AVM), and intracranial aneurysms[34–36] on conventional MRI. Angiography may help distinguish between AVMs and HBs.[36] HBs may also coexist with intracranial aneurysms due to hemodynamic disturbances and chemically modulated mechanisms.[35,36] PAs in adolescents and Mets in adults are important tumors for the differential diagnosis of HBs, namely, cysts with mural nodule type mimics PAs and solid type mimics Mets. Advanced MRI techniques can help

to differentiate PAs and Mets from HBs. HBs often show prominent rCBV values, increased ADC values, and high Lip/Lac without necrosis, while PAs show mildly increased rCBV ratio ranges of 1.40–1.82,[37–39] iso to increased ADC value ranges of $1.11–1.64 \times 10^{-3}$ mm^2/s,[26,37–39] and high Lip/Lac without necrosis.[8,32,33] Finally, Mets show mild to prominent increased rCBV ratio ranges of 2.55–10.80,[9,11,12,40–45] decreased to mildly increased ADC values ranges of $0.79–1.35 \times 10^{-3}$ mm^2/s,[9,11,12,41,42,44] and high Lip/Lac with necrosis.[30,31] The points for differentiation between PAs and Mets from HBs are shown in Table 2.

In our cases, three advanced MRI techniques, namely, DWI, DSC-PWI, and MRS, provided characteristic information that is not available with conventional anatomic MRI alone for the imaging diagnosis of cerebellar HBs. Several studies have evaluated HBs using one of these three advanced MRI techniques,[10,13–15] few studies have evaluated the usefulness of two of the three techniques for differentiating between cerebellar HBs and other cerebellar tumors,[8,9,11,26] and no study has reported whether combining all three advanced MRI techniques could help in diagnosing HBs or more reliably differentiating HBs from other tumors. High ADC, CBV, and Lip/Lac are characteristic findings of cerebellar HBs as described above. These advanced MR imaging findings are useful in more reliable diagnosis as shown in our cases. In addition to conventional anatomical MRI, combining the results from the three advanced MRI techniques may complementarily contribute to a more accurate diagnosis of HBs.

In conclusion, we presented three cases of HBs and reviewed their findings on conventional and advanced MRI, including DWI, DSC-PWI, and MRS. We observed common conventional MR patterns of HBs (cyst with mural nodule type or solid type) in each case. Moreover, solid contrast-enhanced lesions of HBs revealed increased ADC values on DWI, increased rCBV ratios on DSC-PWI, and high Lip/Lac on MRS. Advanced MRI techniques can be helpful in understanding the underlying pathological and metabolic changes of HBs and may be useful for the characterization of HBs by combining results from the three advanced MRI techniques.

Author contributions

Eiji Matsusue performed manuscript writing and contributed to critical revision of the manuscript for important intellectual content.
Chie Inoue and Kensuke Matsumoto contributed to imaging diagnoses of all cases and performed data collection.
Sadaharu Tabuchi, Hiroki Yoshioka, and Yuichiro Nagao contributed to surgical resection and data collection.
Kazuhiko Nakamura performed the project development.
Shinya Fujii gave final approval of the manuscript.
All authors were involved in the revision of the draft manuscript and have agreed to the final content.

ORCID iDs

Eiji Matsusue ⓘ https://orcid.org/0000-0002-0411-1600
Shinya Fujii ⓘ https://orcid.org/0000-0002-0048-0396

References

1. Plate KH, Aldape KD, Vortmeyer AO, et al. Haemangioblastoma. In: Louis DN, Ohgaki H, Wiestler OD, et al (eds) WHO Classification of Tumours of the Central Nervous System. 4th ed. Lyon: International Agency for Research Centre, 2016, pp. 254–257.

2. Hussein MR. Central nervous system capillary haemangioblastoma: the pathologist's viewpoint. Int J Exp Pathol 2007; 88: 311–324.

3. Slater A, Moore NR, Huson SM. The natural history of cerebellar hemangioblastomas in von Hippel-Lindau disease. AJNR Am J Neuroradiol 2003; 24: 1570–1574.

4. Lahkim M, Andour H, Laamrani FZ, et al. Cerebellar hemangioblastoma: case report with review of the literature. Radiol Case Rep 2021; 16: 3109–3112.

5. Hasselblatt M, Jeibmann A, Gerss J, et al. Cellular and reticular variants of haemangioblastoma revisited: a clinicopathologic study of 88 cases. Neuropathol Appl Neurobiol 2005; 31: 618–622.

6. Lee SR, Sanches J, Mark AS, et al. Posterior fossa hemangioblastomas: MR imaging. Radiology 1989; 171: 463–468.

7. Ho VB, Smirniotopoulos JG, Murphy FM, et al. Radiologic-pathologic correlation: hemangioblastoma. AJNR Am J Neuroradiol 1992; 13: 1343–1352.

8. She DJ, Xing Z, Zeng Z, et al. Differentiation of hemangioblastomas from pilocytic astrocytomas using 3-T magnetic resonance perfusion-weighted imaging and MR spectroscopy. Neuroradiology 2015; 57: 275–281.

9. She D, Yang X, Xing Z, et al. Differentiating hemangioblastomas from brain metastases using diffusion-eeighted imaging and dynamic susceptibility contrast-enhanced perfusion-weighted MR imaging. AJNR Am J Neuroradiol 2016; 37: 1844–1850.

10. Quadery FA, Okamoto K. Diffusion-weighted MRI of haemangioblastomas and other cerebellar tumours. Neuroradiology 2003; 45: 212–219.

11. Cha J, Kim ST, Nam DH, et al. Differentiation of hemangioblastoma from metastatic brain tumor using dynamic contrast-enhanced MR Imaging. Clin Neuroradiol 2017; 27: 329–334.

12. Neska-Matuszewska M, Bladowska J, Sasiadek M, et al. Differentiation of glioblastoma multiforme, metastases and primary central nervous system lymphomas using multiparametric perfusion and diffusion MR imaging of a tumor core and a peritumoral zone-Searching for a practical approach. PLoS One 2018; 13: e0191341.

13. Hakyemez B, Erdogan C, Bolca N, et al. Evaluation of different cerebral mass lesions by perfusion-weighted MR imaging. J Magn Reson Imaging 2006; 24: 817–824.

14. Bing F, Kremer S, Lamalle L, et al. [Value of perfusion MRI in the study of pilocytic astrocytoma and hemangioblastoma: preliminary findings]. J Neuroradiol 2009; 36: 82–87.

15. Kumar VA, Knopp EA, Zagzag D. Magnetic resonance dynamic susceptibility-weighted contrast-enhanced perfusion imaging in the diagnosis of posterior fossa hemangioblastomas and pilocytic astrocytomas: initial results. J Comput Assist Tomogr 2010; 34: 825–829.

16. Isobe T, Yamamoto T, Akutsu H, et al. Proton magnetic resonance spectroscopy findings of hemangioblastoma. Jpn J Radiol 2010; 28: 318–321.

17. Mora P, Pons A, Cos M, et al. Magnetic resonance spectroscopy in posterior fossa tumours: the tumour spectroscopic signature may improve discrimination in adults among haemangioblastoma, ependymal tumours, medulloblastoma, and metastasis. Eur Radiol 2019; 29: 2792–2801.

18. Resche F, Moisan JP, Mantoura J, et al. Haemangioblastoma, haemangioblastomatosis, and von Hippel-Lindau disease. Adv Tech Stand Neurosurg 1993; 20: 197–304.

19. Kuharic M, Jankovic D, Splavski B, et al. Hemangioblastomas of the posterior cranial fossa in adults: demographics, clinical, morphologic, pathologic, surgical features, and outcomes. A systematic review. World Neurosurg 2018; 110: 1049–1062.

20. Feletti A, Marrone F, Barresi V, et al. Hemangioblastoma with contrast-enhanced cystic wall: when the surgical rule must not be respected. World Neurosurg 2021; 149: 190–194.

21. Bishop FS, Liu JK, Chin SS, et al. Recurrent cerebellar hemangioblastoma with enhancing tumor in the cyst wall: case report. Neurosurgery 2008; 62: 1378–1379.

22. Sun Z, Yuan D, Sun Y, et al. Surgical resection of cerebellar hemangioblastoma with enhanced wall thickness: a report of two cases. Oncol Lett 2015; 9: 1597–1599.

23. Wang Q, Zhang S, Cheng J, et al. Radiologic features and furgical strategy of hemangioblastomas with enhanced cyst wall. World Neurosurg 2017; 108: 143–150.

24. Utsuki S, Oka H, Sato K, et al. Fluorescence diagnosis of tumor cells in hemangioblastoma cysts with 5-aminolevulinic acid. J Neurosurg 2010; 112: 130–132.

25. Sener RN. Diffusion MRI: apparent diffusion coefficient (ADC) values in the normal brain and a classification of brain disorders based on ADC values. Comput Med Imaging Graph 2001; 25: 299–326.

26. Neska-Matuszewska M, Zimny A, Bladowska J, et al. The role of diffusion and perfusion magnetic resonance imaging in differentiation of haemangioblastomas and pilocytic astrocytomas. Pol J Radiol 2018; 83: 197–203.

27. Onishi S, Hirose T, Takayasu T, et al. Advantage of high b value diffusion-weighted imaging for differentiation of hemangioblastoma from brain metastases in posterior fossa. World Neurosurg 2017; 101: 643–650.

28. Callot V, Galanaud D, Le Fur Y, et al. (1)H MR spectroscopy of human brain tumours: a practical approach. Eur J Radiol 2008; 67: 268–274.

29. Bulik M, Jancalek R, Vanicek J, et al. Potential of MR spectroscopy for assessment of glioma grading. Clin Neurol Neurosurg 2013; 115: 146–153.

30. Poptani H, Gupta RK, Roy R, et al. Characterization of intracranial mass lesions with in vivo proton MR spectroscopy. AJNR Am J Neuroradiol 1995; 16: 1593–1603.

31. Yamasaki F, Takaba J, Ohtaki M, et al. Detection and differentiation of lactate and lipids by single-voxel proton MR spectroscopy. Neurosurg Rev 2005; 28: 267–277.

32. Yue Q, Isobe T, Shibata Y, et al. New observations concerning the interpretation of magnetic resonance spectroscopy of meningioma. Eur Radiol 2008; 18: 2901–2911.

33. Yamasaki F, Takayasu T, Nosaka R, et al. Magnetic resonance spectroscopy detection of high lipid levels in intraaxial tumors without central necrosis: a characteristic of malignant lymphoma. J Neurosurg 2015; 122: 1370–1379.

34. Murai Y, Kobayashi S, Tateyama K, et al. Persistent primitive trigeminal artery aneurysm associated with cerebellar hemangioblastoma. Case Report. Neurol Med Chir (Tokyo) 2006; 46: 143–146.

35. de San Pedro JR, Rodríguez FA, Níguez BF, et al. Massive hemorrhage in hemangioblastomas Literature review. Neurosurg Rev 2010; 33: 11–26.

36. Wang Z, Hu J, Xu L, et al. Intratumoral hemorrhage in a patient with cerebellar hemangioblastoma: a case report and review. Medicine (Baltimore) 2015; 94: 497.

37. de Fatima Vasco Aragao M, Law M, Batista de Almeida D, et al. Comparison of perfusion, diffusion, and MR spectroscopy between low-grade enhancing pilocytic astrocytomas and high-grade astrocytomas. AJNR Am J Neuroradiol 2014; 35: 1495–1502.

38. Kikuchi K, Hiwatashi A, Togao O, et al. Usefulness of perfusion- and diffusion-weighted imaging to differentiate between pilocytic astrocytomas and high-grade gliomas: a multicenter study in Japan. Neuroradiology 2018; 60: 391–401.

39. Ho CY, Supakul N, Patel PU, et al. Differentiation of pilocytic and pilomyxoid astrocytomas using dynamic susceptibility contrast perfusion and diffusion weighted imaging. Neuroradiology 2020; 62: 81–88.

40. Hakyemez B, Erdogan C, Gokalp G, et al. Solitary metastases and high-grade gliomas: radiological differentiation by morphometric analysis and perfusion-weighted MRI. Clin Radiol 2010; 65: 15–20.

41. Gaudino S, Di Lella GM, Russo R, et al. Magnetic resonance imaging of solitary brain metastases: main findings of nonmorphological sequences. Radiol Med 2012; 117: 1225–1241.

42. Tsougos I, Svolos P, Kousi E, et al. Differentiation of glioblastoma multiforme from metastatic brain tumor using proton magnetic resonance spectroscopy, diffusion and perfusion metrics at 3 T. Cancer Imaging 2012; 12: 423–436.

43. Bauer AH, Erly W, Moser FG, et al. Differentiation of solitary brain metastasis from glioblastoma multiforme: a predictive multiparametric approach using combined MR diffusion and perfusion. Neuroradiology 2015; 57: 697–703.

44. Usinskiene J, Ulyte A, Bjornerud A, et al. Optimal differentiation of high- and low-grade glioma and metastasis: a meta-analysis of perfusion, diffusion, and spectroscopy metrics. Neuroradiology 2016; 58: 339–350.

45. Li X, Wang D, Liao S, et al. Discrimination between glioblastoma and solitary brain metastasis: comparison of inflow-based vascular-space-occupancy and dynamic susceptibility contrast MR imaging. AJNR Am J Neuroradiol 2020; 41: 583–590.